High-heat-flux rectification due to a localized thermal diode

Tristram J. Alexander*
School of Physics, University of Sydney, Sydney, New South Wales 2006, Australia

(Received 17 February 2020; accepted 14 April 2020; published 15 June 2020)

A theoretical implementation of a localized thermal diode with a rectification factor greater than 10^6 is demonstrated. In reverse thermal bias, extremely low thermal conductivity is achieved through phononic Rayleigh scattering from a finite-depth defect. In forward bias, the diode oscillator escapes the defect and thermal conductivity becomes up to four orders of magnitude higher. The setup provides a minimal model of a localized thermal diode between two identical oscillator chains and opens up a pathway for thermal diode implementations.

DOI: 10.1103/PhysRevE.101.062122

I. INTRODUCTION

The control of heat at the nanoscale is a highly active research area, for its promise in thermoelectric energy harvesting [1] and heat-flow management [2]. Of particular interest for these applications is the development of a "thermal diode," a device which has either high or low thermal conductivity, depending on the direction of heat flow [3,4]. The search for such a device has relied heavily on idealized models of materials, based on oscillator chains, to allow the essential physics to be uncovered [5]. One of the first works in this direction showed that thermal diodelike behavior could be obtained by using two different chains of oscillators, relying on a bulk transition to nonlinear behavior in one of the chains [6,7]. Unfortunately, this reliance on the nonlinear properties of the chain meant that the observed thermal rectification effects disappeared with increasing chain length, as far from a thermal bath the oscillator chain would revert to linear behavior [8]. A recent approach has sought to circumvent this problem by considering only short nonlinear chains, separated by a long linear chain [9]. However, as the linear chain shows no thermal gradient (and therefore does not follow the Fourier heat diffusion law [10,11]), the underlying problem of the size dependent thermal rectification is sidestepped rather than confronted.

In this work, I show that thermal diode effects may be achieved by introducing a single-site defect with asymmetric coupling (see Fig. 1). The key thermal conduction effects are confined to the defect, which means there is no need for a bulk temperature-dependent thermal conductivity, or the need for two different materials. A recent work has demonstrated thermal rectification effects due to a soft-wall localized impurity between two identical oscillator chains [12]; however, with no temperature-dependent transition between a low- and high-conducting state, the resulting rectification is weak and disappears for a longer chain. In this work, I show that temperature-dependent conduction underpins strong rectification and demonstrate that this may be achieved with a localized defect.

The general requirement of asymmetry and nonlinearity for thermal rectification has been established theoretically [13,14], although it should be noted that these conditions are necessary but not sufficient [15]. Early work identified that asymmetry between a two-state quantum system and thermal baths could lead to thermal rectification [16,17]. In this work, I demonstrate analogous two-state-like effects in an entirely classical system.

Experimental examples of systems with asymmetry and a temperature-dependent conductivity abound, including graded masses in a carbon nanotube [18], mercury in a vertical cylinder [19], phase change materials in an asymmetric configuration [20,21], and structural detuning in the presence of radiation [22]. The idealized model presented in this work provides a minimal theoretical model for capturing and describing these effects.

The work proceeds as follows. In Sec. II, I introduce the theoretical model used to describe the thermal diode. In Sec. III, I introduce the numerical approach and diode metrics, and demonstrate the essential function of the thermal diode. In Sec. IV, I introduce a simple coupled oscillator model to describe the diode action and find an analytical expression for the dependence of the flux on the diode parameters. In Sec. V, I check the analytical predictions with a numerical study of the flux dependence. In Sec. VI, I examine the dependence of the diode behavior on chain length. In Sec. VII, I provide some physical estimates of diode operation, while in Sec. VIII, I provide some final conclusions.

II. MODEL

The model seeks to describe two identical materials [shown schematically in Fig. 1(a)], using a simple oscillator model [see Fig. 1(b)]. In this work, I focus on the one-dimensional Frenkel-Kontorova model [23], which, with its local on-site potential, provides a highly simplified model of mechanical vibrations in a crystalline solid. As I will show, high rectification in this system may be achieved by using a local finite-depth defect in the presence of asymmetric coupling [see Fig. 1(c)]. The defect is shown to locally decouple the phonon bands [Fig. 1(e)], leading to effective phonon Rayleigh scattering and, consequently, very low thermal conductivity. However, above a critical local temperature, the diode

*tristram.alexander@sydney.edu.au

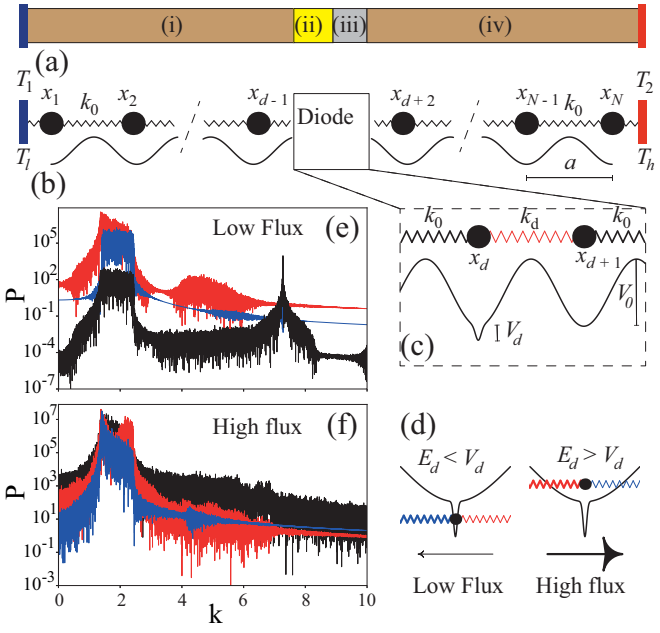

FIG. 1. (a) Thermal diode configuration: (i) and (iv) represent identical materials separated by (ii) a material with a temperature-dependent phonon spectrum and (iii) a low thermal conductivity material. (b) Schematic of oscillator chain capturing the behavior in (a) (shown in reverse-bias configuration) with (c) details of the diode showing the presence of a defect (leading to temperature-dependent phonon spectrum) and asymmetric coupling into the defect. (d) Left: When the oscillator is confined to the the defect, the oscillator frequency does not overlap with the phonon bands (e), and there is low flux. (d) Right: When the oscillator escapes the defect, it overlaps with the phonon bands (f), and there is high flux. (e),(f) Fourier power spectra for $T_l = 0.05$, $T_h = 0.6$ in reverse- and forward-bias configurations, respectively. For both, $k_d = 0.2$. Lines correspond to spectra for the defect oscillator (black) and nearest neighbors (red and blue), with red the oscillator on the high temperature side and blue the oscillator on the low temperature side.

oscillator escapes the defect [Fig. 1(d)], leading to phonon band overlap [Fig. 1(f)] and high thermal conductivity. The required nonlinear thermal response is thus contained simply in the finite depth of the defect. Asymmetric coupling into the defect means that escape (and, thus, high thermal conductivity) depends on both the temperature and the direction of the thermal gradient.

In the general case, I will consider a one-dimensional model of a chain of particles of mass $\tilde{m}$ harmonically coupled to their immediate neighbors through linear springs and located on a substrate potential $\tilde{V}_s$. For the majority of this work, I shall restrict attention to the specific case of the Frenkel-Kontorova model [23], for which the substrate potential is sinusoidal with depth $\tilde{V}_0$ and period $\tilde{a}$ [see Figs. 1(a) and 1(b)]. To this model, I add a Gaussian defect potential, localized on a single site $i = d$, characterized by depth $\tilde{V}_d$ and inverse width constant $\tilde{w}_d$ [see Fig. 1(c)]. The Hamiltonian for this system takes the form

$$\mathcal{H} = \sum_{i=1}^{N}\left[\frac{\tilde{p}_i^2}{2\tilde{m}} + \tilde{V}_s(\tilde{q}_i) + \frac{1}{2}\tilde{k}_i(\tilde{q}_{i+1} - \tilde{q}_i)^2\right] + \tilde{V}_d \exp\left(-\tilde{w}_d^2\tilde{q}_d^2\right), \quad (1)$$

where $\tilde{q}_i$ and $\tilde{p}_i$ are the displacement from equilibrium and the associated momentum for the ith particle, respectively, and $\tilde{k}_i = \tilde{k}_0$ for all i except $i = d$. At the defect, coupling between the dth and $(d+1)$th particle is set to $\tilde{k}_d$, thus breaking the left-right symmetry of the chain, which is a fundamental requirement for the observation of rectification effects [13,14]. With $\tilde{k}_d \ll \tilde{k}_0$, this simulates the low thermal conductivity region (iii) shown in Fig. 1(a). For the specific case of the Frenkel-Kontorova model, $\tilde{V}_s(\tilde{q}_i) = \tilde{V}_0[1 - \cos(\frac{2\pi}{\tilde{a}}\tilde{q}_i)]$. In Sec. VI, I will also consider a quartic potential $\tilde{V}_s(\tilde{q}_i) = \tilde{V}_0\tilde{q}_i^2 + \tilde{V}_n\tilde{q}_i^4$.

The equations of motion for the oscillators follow from Hamilton's equations, $\dot{\tilde{q}}_i = \frac{\partial H}{\partial \tilde{p}_i}$ and $\dot{\tilde{p}}_i = -\frac{\partial H}{\partial \tilde{q}_i}$. For the Frenkel-Kontorova model, the resulting second-order equation for the displacement $\tilde{q}_i$ is

$$\ddot{\tilde{q}}_i = -\frac{2\pi}{\tilde{m}\tilde{a}}\tilde{F}_s\left(\frac{2\pi}{\tilde{a}}\tilde{q}_i\right) + \frac{\tilde{k}_i}{\tilde{m}}\tilde{q}_{i+1} + \frac{\tilde{k}_{i-1}}{\tilde{m}}\tilde{q}_{i-1} - \left(\frac{\tilde{k}_i}{\tilde{m}} + \frac{\tilde{k}_{i-1}}{\tilde{m}}\right)\tilde{q}_i - \frac{2\tilde{V}_i}{\tilde{m}}\tilde{w}_d^2\tilde{q}_i \exp\left(-\tilde{w}_d^2\tilde{q}_i^2\right), \quad (2)$$

where $\tilde{F}_s(\frac{2\pi}{\tilde{a}}\tilde{q}_i) = \tilde{V}_0 \sin(\frac{2\pi}{\tilde{a}}\tilde{q}_i)$, and $\tilde{V}_{i\neq d} = 0$, $\tilde{V}_{i=d} = \tilde{V}_d$. Note that the tilde sign has been used to indicate quantities with dimensions.

A dimensionless model can be obtained through the following transformations: $x_i = (2\pi/\tilde{a})\tilde{q}_i$ and $t = (2\pi/\tilde{a})\sqrt{\tilde{V}_0/(\tilde{m}V_0)}\tilde{t}$, where V_0 is a dimensionless scaling constant. The equation of motion for the ith particle in the Frenkel-Kontorova model is then given by

$$\ddot{x}_i = -F_s(x_i) + k_i x_{i+1} + k_{i-1}x_{i-1} - (k_i + k_{i-1})x_i - V_i w_d^2 x_i \exp\left(-w_d^2 x_i\right), \quad (3)$$

where now $F_s(x_i) = V_0 \sin(x_i)$. In terms of the original physical quantities, the dimensionless parameters are $V_d = 2V_0\tilde{V}_d/\tilde{V}_0$, $w_d^2 = \tilde{w}_d^2\tilde{a}^2/(2\pi)^2$, and $k_i = (V_0\tilde{a}^2/(4\pi^2\tilde{V}_0))\tilde{k}_i$.

The chain is extended at either end by N_t particles (in practice, $N_t = 10$) to provide a thermal bath. Each particle in the thermostat chain obeys (3), while also coupled to a Nosé-Hoover thermostat [24]. The thermostat response time is taken to be 1. The chain on the left (coupling to the $i = 1$ particle) is held at temperature T_1, while the chain on the right (coupling to the $i = N$ particle) is held at temperature T_2. In the normalized model, the local definition of temperature [24] is given simply by the local time average of the square of the velocity: $T_i = \langle \dot{x}_i^2 \rangle$.

There are two significant features in this model relative to earlier work: a temperature-dependent phonon spectrum due to the narrow on-site Gaussian defect, and the presence of an identical potential depth V_0 for all particles (without loss of generality, I take $V_0 = 2$). This simulates the case of identical materials (i) and (iv) in Fig. 1(a). The majority of the analysis in this work is conducted for a chain of length $N = 102$, with the defect located at the center of the chain ($i = d = 51$).

Throughout this work the lower temperature is fixed at $T_l = 0.05$. In the forward-bias configuration, $T_2 = T_l$, and the reverse-bias corresponds to $T_1 = T_l$ [reverse bias is shown in Figs. 1(a) and 1(b)].

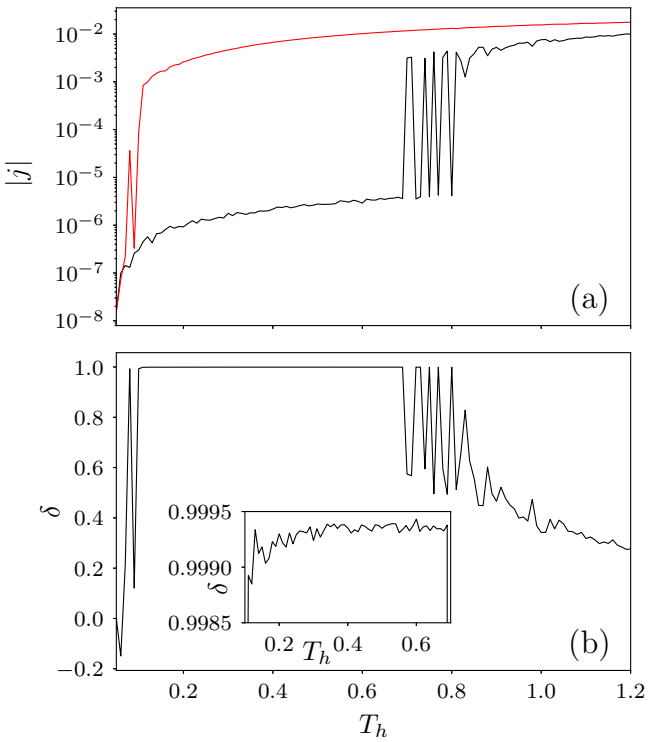

FIG. 2. (a) Flux through diode in forward- (red) and reverse- (black) bias configurations as a function of T_h. (b) Diodicity, showing the region where diodicity is close to 1 (inset). Other parameters are $T_l = 0.05$, $k_d = 0.2$, $V_d = 0.25$, $w_d = \sqrt{200}$, and $N = 102$.

III. THERMAL DIODE OPERATION

I begin by examining the heat flux through the chain for different thermostat temperatures. Fixing the lower temperature to be $T_l = 0.05$, the upper temperature T_h is varied. Following the derivation presented in [24], the local heat flux is

$$j_i = \frac{k_i}{2}(\dot{x}_{i+1} + \dot{x}_i)(x_{i+1} - x_i). \tag{4}$$

The time average of (4) is found by allowing the system to first evolve for $t = 10^7$ time units and the local flux is then averaged over the following $t = 2 \times 10^7$ time units. Except for the longer chains considered later in this work, this is sufficient for the local flux to be uniform across the chain, such that a single flux value $j(=j_i)$ can be used to characterize the flux. The majority of the analysis in this work is conducted for a chain of length $N = 102$, with the defect and its asymmetrically coupled neighbor located at the center of the chain ($i = d = 51$). All time integration is carried out using the fourth-order Runge-Kutta algorithm with a time step $\Delta t = 0.005$.

Setting $V_d = 0.25$ and $k_d = 0.2$, we see, in Fig. 2, evidence of thermal diode behavior. In the forward-bias configuration (red line), the heat flux is initially low for small T_h, but for $T_h \geqslant 0.13$, a large heat flux occurs. This is the diode turn-on temperature. The oscillator escapes the defect and its spectral response overlaps strongly with both chains [Figs. 1(c) and 1(e)]. Beyond this turn-on temperature, the heat flux increases almost linearly with temperature. With the thermostats in the reverse-bias configuration, high thermal flux requires much higher temperatures, with the reverse-bias turn-on temperature (and thus the thermal diode breakdown temperature) $T_h = 0.7$. In the temperature range $T_h \in [0.13, 0.69]$, the flux is three orders of magnitude lower in the reverse-bias configuration than in the forward-bias configuration. In this regime, the oscillator is confined to the defect and has only weak spectral overlap with the chains on either side [Figs. 1(c) and 1(d)]. The asymmetry in the heat flux can be characterized through the rectification coefficient,

$$R = (|j^+| - |j^-|)/|j^-|, \tag{5}$$

and the diodicity,

$$\delta = \frac{|j^+| - |j^-|}{|j^+| + |j^-|}, \tag{6}$$

where j^+ and j^- are the observed fluxes in the forward- and reverse-bias configurations, respectively. To be consistent with the electronics formalism, we use δ [3]; however, where necessary to compare with previous results, we calculate R. We can see in Fig. 2(b) that the diodicity is above 0.999 across the range of operation (where a perfect diode has $\delta = 1$).

We can summarize the diode operation requirements as follows: T_h needs to be sufficient to allow the oscillator to escape when in forward bias, but insufficient for escape when in reverse bias. Similarly, T_l must be low enough such that the oscillator is trapped by the defect in the reverse-bias configuration. This introduces constraints on the thermal operating range of the diode.

For lower T_l, there will be little change in the bounds. For higher T_l, particularly a T_l approaching the breakdown of the diode in reverse bias, the T_h turn-on temperature will be lower, but the upper cutoff temperature will be lower too, so that overall the operating range will decrease.

IV. PHONONIC RAYLEIGH SCATTERING

To identify the dependence of the flux on the defect parameters when the oscillator is confined to the defect, we reduce the problem to three linear oscillators with positions $[x_1, x_2, x_3]$ and associated harmonic trap frequencies $[\omega_0, \omega_d, \omega_0]$. Oscillator 1 couples to oscillator 2 through a linear spring with spring constant k, while oscillator 2 is coupled to oscillator 3 with linear spring k_d. We see that the normal modes in this system become localized on each oscillator in the limit $\omega_d \gg \omega_0$, $k_d \ll k$, with mode frequencies $\omega_1 = \sqrt{\omega_0^2 + k}$, $\omega_2 = \sqrt{\omega_d^2 + k + k_d}$, and $\omega_3 = \sqrt{\omega_0^2 + k_d}$. We can make a quantitative estimate of the effective coupling between the end oscillators by examining the initial value problem in which all oscillators are initially at rest and only x_1 is displaced, with $x_1 = x_{\text{init}}$. Solving this initial value problem in the limit $\omega_d \gg \omega_0$, $k_d \ll k$, we find that the maximum amplitude of x_3 takes the form

$$x_{3_{\max}} = \frac{2kk_d x_{\text{init}}}{\omega_d^2(k - k_d)}. \tag{7}$$

This approximation can give an estimate of the maximum flux passing through the defect from one end oscillator to the other.

We know from the solution to the initial value problem that energy will be exchanged between the end oscillators

with a frequency given by $(\omega_1 - \omega_3)/2$. Taking the flux to therefore be a sinusoidal function at twice this frequency, $J = J_{amp}\sin(\omega_1 - \omega_3)t$, we can estimate the maximum flux to be

$$J_{amp} = \frac{1}{4}x_{3_{\max}}^2\left(\omega_0^2 + k_d\right)\left(\sqrt{\omega_0^2 + k} - \sqrt{\omega_0^2 + k_d}\right) \quad (8)$$

$$\approx \frac{kk_d^2x_i^2\omega_0}{2\omega_d^4}. \quad (9)$$

As this assumes a smooth sinusoidal exchange of energy, we expect it will underestimate the maximum flux values found in the system, as the flux averaged over one oscillator period will show large fluctuations, due to the influence of the defect oscillator. This is indeed what we observe when we compare the analytical predictions with the numerically calculated maxima; however, the overall dependence shows the $1/\omega_d^4$ flux dependence predicted. It should be noted that this flux dependence breaks down if only one symmetry is broken (i.e., when either $k_d = k$ or $\omega_d = \omega_0$), in which case the end oscillators are always coupled through the normal modes.

Returning to the full system, we see in Fig. 3(a) that the flux through the diode does indeed go as $1/\omega_d^4$. The dotted line is the fitting function $0.008125/\omega_d^4$, where $\omega_d^2 = w_d^2V_d$ is the linear trap frequency for the defect in the limit of small oscillations. This dependence is consistent with phononic Rayleigh scattering, as expected for a defect of much smaller size than the average phonon wavelength. While the flux in the reverse-bias configuration is decreasing with frequency (above some critical ω_d), the flux in the forward-bias configuration is unchanged, as expected for a defect which is a small perturbation after escape. The consequence of this is that the diodicity steadily increases. At $\omega_d = 10$, we have $\delta = 0.99985$, which corresponds to a rectification factor $R = 1.38 \times 10^6$. This is significantly higher than previously reported values [4,6,7,9,12,25].

V. DEFECT-MEDIATED DYNAMICS

As the defect frequency is decreased in the reverse-bias configuration, we see in Fig. 3(a) a sudden jump to higher flux below a critical frequency. At this frequency, the diode oscillator is able to escape the defect, resulting in stronger coupling across the diode and, thus, diode breakdown. The study of thermally activated escape is an extensive and active area (see, e.g., [26] for a recent review); however, the problem here is further complicated by the continuing interaction of the oscillator with the defect. The possibility of defect escape and recapture leads to a noisy transition to diode breakdown, as seen in the jumps to and from high flux in Fig. 2. Solving this problem is beyond the scope of this work; however, we can make some scaling estimates and identify some of the breakdown pathways. At large ω_d, escape occurs when the energy in the linear spring, coupling the defect to one of the chains, is close to V_d. In this static picture, we can obtain an estimate of the diode oscillator escape temperature by assuming that the oscillator at temperature T moves with average amplitude sufficient for this temperature at the minimum oscillation frequency $\sqrt{V_s}$, yielding $A = \alpha\sqrt{2T/V_s}$. In practice, the thermal fluctuations around this average imply the maximum amplitude must be significantly higher than this, i.e., $\alpha > 1$. Equating the energy in the spring at the amplitude A, $E_{\text{spring}} = \frac{1}{4}k_dA^2$ to some fraction of the depth of the defect $E_{\text{defect}} = \beta V_d$, we obtain the critical escape temperature $T_{cr} = V_sV_d/(\gamma k_d)$, where $\gamma = \alpha^2/\beta$. As the frequency of the oscillator in the defect decreases with increasing energy, overlap may occur before the particle completely escapes, so we take $\beta < 1$. Taking physically reasonable values, $\alpha = 1.5$ and $\beta = 0.75$ yields $\gamma = 3$. In forward bias with $V_d = 0.25$, the predicted transition from bound to free occurs at $T_{cr} = 0.17$. This compares with the numerically obtained value of $T_{cr} = 0.1$ found in Fig. 2. We show in Fig. 3(b) the dependence of flux on T_h in the reverse-bias configuration for $k_d = [0.1, 0.2, 0.3, 0.4, 0.5]$. The prediction captures the key behavior, but appears to overestimate the breakdown temperature. The reason for the overestimation

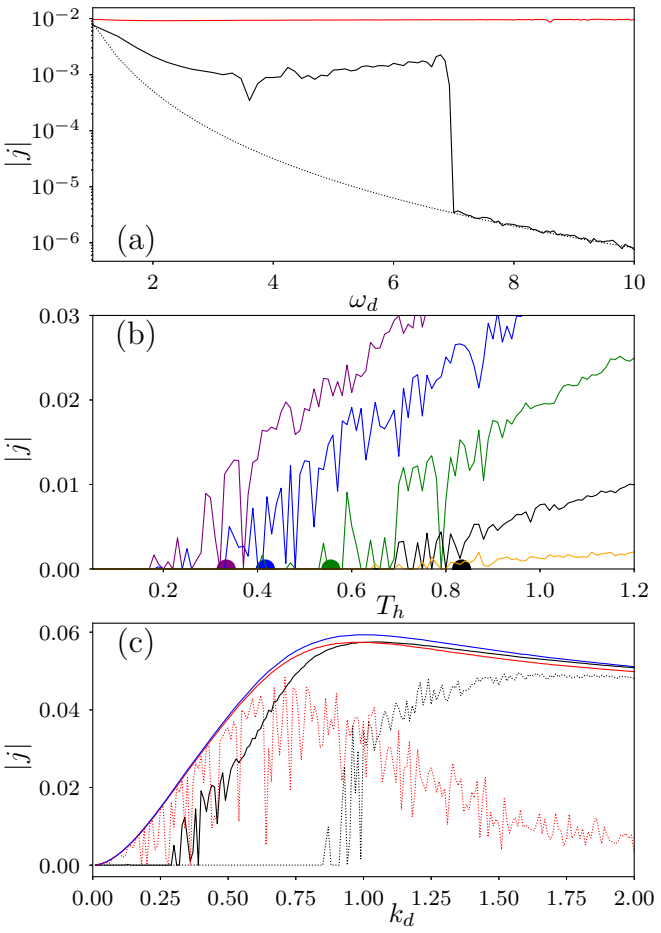

FIG. 3. (a) Dependence of flux on linear frequency of defect. Parameters: $T_h = 0.4$, $T_l = 0.05$; $V_d = 0.25$. (b) Dependence of flux on temperature in reverse-bias configuration, showing the $1/k_d$ dependence of the breakdown temperature. Lines from top to bottom are $k_d = 0.5$ (purple), $k_d = 0.4$ (blue), $k_d = 0.3$ (green), $k_d = 0.2$ (black), and $k_d = 0.1$ (orange). Half circles are the corresponding analytical breakdown predictions. (c) Dependence of flux on k_d at $T_h = 0.6$. Blue line: $V_d = 0$, showing maximum flux. Solid lines: $V_d = 0.25$. Dashed lines: $V_d = 0.5$. Red: forward bias; black: reverse bias.

is that when the defect frequency and phonon band become closer, dynamical effects come into play [as evident in the frequency dependence of Fig. 3(a)], so we expect the static approach will always overestimate the critical temperature. The estimate for $k_d = 0.1$ is particularly poor as at high temperature the phonon band of the oscillator chain has spread sufficiently to weakly couple with the defect, so flux occurs even without the oscillator leaving the defect.

We consider now the maximum flux possible in the system. In the absence of any defect, we have two identical chains with some interfacial coupling. This serves as the maximum available flux in the system [blue line in Fig. 3(c)] and peaks at $k_d = 1$ (similar results have been observed between two different chains [8]). For $V_d = 0.25$ [solid red (forward) and black (reverse) in Fig. 3(c)], we see a critical coupling strength of $k_{d_{cr}} = 0.33$, beyond which the diode breaks down. Increasing the defect depth to $V_d = 0.5$, we see this critical coupling strength increases to $k_{d_{cr}} = 0.91$. While this is consistent with the critical escape temperature behavior identified in the previous paragraph, it also continues to illustrate the deviation from the predicted linear behavior. The implication of the result is the possibility for significant flux in the forward bias with negligible flux in the reverse bias, provided $k_d < k_{d_{cr}}$. However, the flux in the $V_d = 0.5$ case is noisy due to the continued interaction of the oscillator with the defect. At $k_d = 0.5$, we see $\delta = 0.99968$, but the forward flux is more than three times that observed for $k_d = 0.2$. For $k_d > 1$, we see that the diode bias directions are reversed, though the diodicity is low, $\delta < 0.5$.

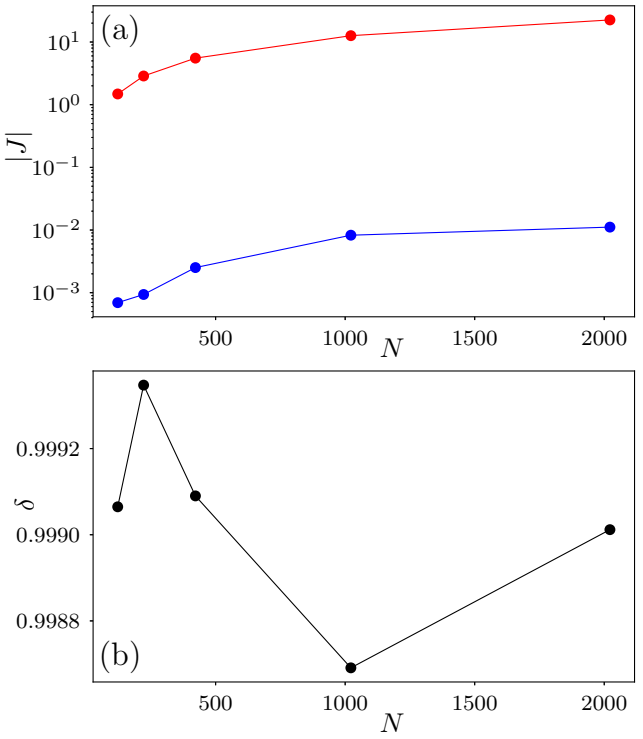

FIG. 4. (a) Dependence of total flux $J = Nj$ on chain length for forward bias (red) and reverse bias (blue) for the Frenkel-Kontorova model, showing increase in flux with chain length. (b) Diodicity is almost constant with length.

VI. LENGTH DEPENDENCE OF THERMAL RECTIFICATION

Thermal rectification in Frenkel-Kontorova (FK) chains has in the past relied on a bulk transition in the phonon spectrum, due to the nonlinear nature of the substrate potential. This approach has suffered from a decrease, and even possible reversal, in diodicity due to the decrease in effective nonlinearity far from the thermal source [8]. Practically, this means diodicity in the two-chain system depends strongly on chain length. Similarly, for the case of the one-sided "soft-wall" defect introduced in Ref. [12], the thermal rectification coefficient is found to decay from $R = 0.31$ at $N = 20$ (corresponding to a diodicity of $\delta = 0.13$) to $R = 0.178$ at $N = 150$, thus also showing a decrease in effectiveness with length. It is therefore important to consider the effect of chain length for the case of a single-site defect.

In Fig. 4, we can see the effects of increasing chain length. In Fig. 4(b), we see that while there is some variation of the diodicity around $\delta = 0.999$, there is no systematic decrease with length. However, the calculated fluxes shown in Fig. 4(a) indicate that the total flux $J = Nj$ is increasing with chain length. As thermal conductivity is given by $\kappa = J/(T_h - T_l)$, this result suggests that thermal conductivity is increasing with length.

Thermal conductivity in a Frenkel-Kontorova lattice has been found to asymptotically tend to a finite value with increasing chain length [27,28]; however, a number of difficulties with calculating values for a thermal conductivity in nonlinear lattices have been identified [24]. For the temperatures used in the creation of Fig. 4, the lattice appears to be in a predominantly linear regime, which is in stark contrast to the highly nonlinear regime used in the past to find a finite value for the thermal conductivity [28]. It may simply be that thermalization is extremely slow, or the convergence to a finite thermal conductivity only becomes evident at a much longer chain length; however, either way there is some subtlety in the nature of thermal conductivity in FK lattices. Further investigation is beyond the scope of this work.

Instead, to verify that the diode effects observed in FK lattices persist when thermal equilibrium can be assured, I turn to a ϕ^4 lattice, which functionally looks like the Frenkel-Kontorova lattice truncated at the first nonlinear term. Specifically, I consider the confining quartic potential given in Sec. II. The equations of motion are still given by Eq. (3), but now $F(x_i) = V_0 x_i + V_n x_i^3$. Inspired by the observations of the failings in the Frenkel-Kontorova model, I consider a strongly nonlinear restoring force, with $V_0 = 1$ and $V_n = 10$. Similarly, to ensure that we are in the nonlinear regime, I set $T_l = 0.5$ and $T_h = 1.5$.

Proceeding with analogous numerical simulations to those conducted for the FK model, we see that the diodicity in Fig. 5(b) continues to show no systematic change with length, but now the flux in the forward and reverse directions shown in Fig. 5(a) assumes an asymptotic value, indicating a well-defined thermal conductivity. There has been no attempt to optimize this configuration for high thermal rectification, yet we see that the diodicity is still fluctuating around $\delta = 0.995$. The underlying mechanism of the rectification thus appears to

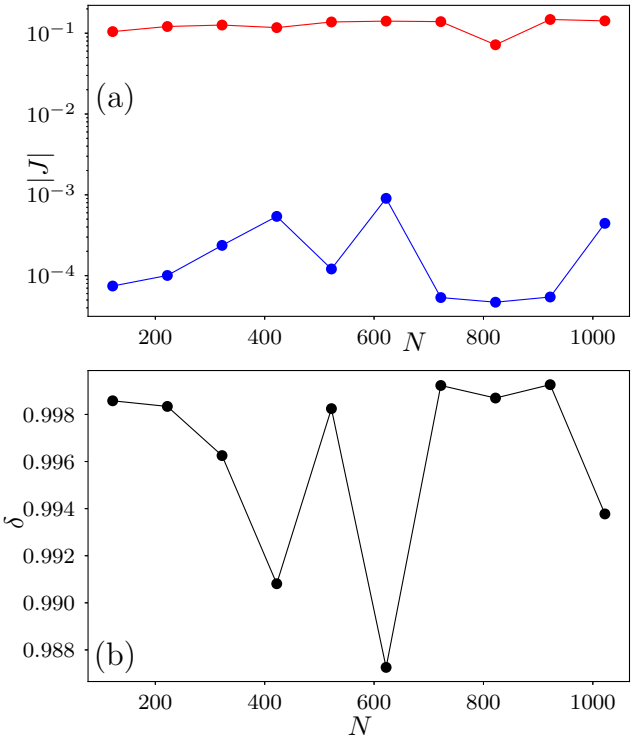

FIG. 5. (a) Dependence of total flux $J = Nj$ on chain length for forward bias (red) and reverse bias (blue) for the ϕ^4 model, showing an almost constant total flux. (b) Diodicity shows no systematic change with length.

be robust against changes in the details of the oscillator chain. Operation of the diode proceeds, provided the frequency of the diode potential is well removed from the bulk phonon spectrum in the chain.

VII. PHYSICAL CONSIDERATIONS

This work has explored the theoretical implications of a localized defect in a Frenkel-Kontorova chain. In this section, I will look at possible physical implementations of this system. The key considerations are the temperatures involved, the validity of the classical approach, and the physical characteristics of the defect. As we shall see, these factors place significant constraints on a possible experimental implementation of a thermal diode based on a localized defect.

Throughout this work, I have used dimensionless temperatures, so a first step is to convert the normalization to physical values. To this end, the equipartition theorem of classical statistical mechanics is applied [4], which for the single degree-of-freedom oscillator chain considered here gives

$$\frac{1}{2}k_B\tilde{T} = \frac{1}{2}\tilde{m}\langle\dot{\tilde{q}}_i^2\rangle = \frac{1}{2}\tilde{m}\left(\frac{\tilde{V}_s}{\tilde{m}V_0}\right)\langle\dot{x}_i^2\rangle = \frac{1}{2}\frac{\tilde{V}_s}{V_0}T, \tag{10}$$

where I have made use of the scaling relations between dimensionless and physical variables introduced in Sec. II, and k_B is the Boltzmann constant. We thus obtain a relatively simple relation between the real temperature $\tilde{T}$ and the normalized temperature T,

$$\tilde{T} = \frac{\tilde{V}_s}{k_B V_0}T, \tag{11}$$

where, due to the scaling relations employed in the derivation of the normalized model (3), the conversion is determined by the single free physical parameter $\tilde{V}_s$. This single parameter determines the energy scale of the nonlinearity in the Frenkel-Kontorova model (1). A similar approach is used in Ref. [28], where instead three physical parameters are used to characterize the physical regime of operation.

To determine the validity of the classical approach to the defect dynamics, we must compare the defect depth $\tilde{V}_d$ with the characteristic energy scale $\hbar\tilde{\omega}_d$ of a quantum harmonic oscillator in the defect. To this end, I introduce a dimensionless parameter γ to quantify the relation between the energy scales, with $\gamma \gg 1$ corresponding to a valid classical implementation of the defect,

$$\gamma = \frac{\tilde{V}_d}{\hbar\tilde{\omega}_d} = \frac{\tilde{a}}{2\pi}\sqrt{\frac{\tilde{m}V_0}{\tilde{V}_s}}\frac{\tilde{V}_d}{\hbar\omega_d} = \frac{\tilde{a}}{2\pi}\sqrt{\frac{\tilde{m}\tilde{V}_s}{2V_0}}\frac{V_d}{\hbar\omega_d}, \tag{12}$$

where I have made use of the temporal dimensionless scaling in Sec. II.

Finally, we need a physical measure of the defect size. The physical full width at half maximum is given by

$$\tilde{q}_{fwhm} = \frac{\sqrt{\ln 2}}{\tilde{w}_d} = \frac{\sqrt{\ln 2}\tilde{a}}{2\pi w_d} = \frac{\sqrt{V_d \ln 2}}{2\pi\omega_d}\tilde{a}, \tag{13}$$

where again I have made use of the scaling relations in Sec. II. We see that for $V_d = 0.25$ and $\omega_d = 8$, this leads to a relationship of $\tilde{q}_{fwhm} \approx 0.008\tilde{a}$. With Eqs. (11)–(13), we are thus able to determine the validity and accessibility of the predicted effects in various physical systems.

A defect of less than 1% of the interoscillator distance rules out this approach for any regular material. This is compounded by the fact that $\hbar\tilde{\omega}_d \sim k_B\tilde{T}$ for defects of this scale in a typical crystal. For instance, for carbon atoms in graphene, $\gamma \approx 0.25$, meaning quantum effects need to be taken into account in any complete treatment, while $\tilde{q}_{fwhm} \approx$ 1 pm puts the requirements of the defect beyond current technical capabilities.

To observe the effects predicted in this work therefore requires much larger spatial scales. Ion Coulomb crystals provide one possible physical testbed. Looking at the experimental work of Ref. [29], for instance, we can see for an ion crystal of barium-138, $\tilde{V}_s \approx 50$ mK $\times k_B$, $\tilde{a} \approx 35$ μm, and $\tilde{m} \approx 2.3 \times 10^{-25}$ kg. In this case, the classical to quantum ratio is $\gamma \approx 300$, so with $\gamma \gg 1$ the classical approach used in this work is valid. The size of the defect, $\tilde{q}_{fwhm} = 300$ nm, is possible to achieve optically, so it is compatible with the optical techniques underpinning ion Coulomb crystals. Finally, the asymmetric coupling necessary for the thermal diode operation may be achieved by introducing an empty site in the one-dimensional ion crystal chain. With the defect located on an oscillator next to the empty site, the coupling across the empty site will be weaker than the coupling to an immediate neighbor. The physical temperatures involved for $T_h = 0.6$ and $T_l = 0.05$ will be $\tilde{T}_h \approx 15$ mK and $\tilde{T}_l \approx 1$ mK, both well below T_c for the ion crystal. Such a system has the added advantage that it is well approximated by a one-dimensional chain in a periodic potential.

An interesting question is how the results presented in this work may be extended to higher-dimensional systems.

There is nothing that intrinsically prevents this. With a similar increase in the dimensionality of the defect, the results presented here will have direct physical parallels with the higher-dimensional versions. The technical challenge is to create two-dimensional (or three-dimensional) finite-depth defects. For instance, in the case of a physical ribbon-type geometry, each oscillator in a short cross section of the ribbon would need to be located on a defect.

VIII. CONCLUSION

This work has shown that within the formalism of a nonlinear oscillator chain, a thermal diode with a high rectification factor can be achieved through a finite-depth defect and asymmetric coupling. High diodicities, greater than 0.999, are demonstrated and the effects are shown to persist as the length of the chain is increased. The approach used is a significant departure from the typical implementation relying on nonlinear behavior in a bulk chain to achieve rectification. Here, the bulk chains are in the linear regime, and as such can be identical. All of the nonlinear, temperature-dependent effects are contained in the localized defect. Indeed, the largely linear chain behavior likely underpinned the absence of convergence to a finite thermal conductivity. The robustness of the thermal diode operation was, however, demonstrated by placing the diode in a highly nonlinear ϕ^4 chain, and showing similar levels of diodicity.

This work outlines a simple approach for achieving thermal rectification; however, it also identifies a number of possible subtleties inherent in using nonlinear oscillator chains to model heat transport. The Frenkel-Kontorova model appears to display anomalous heat diffusion when in the linear regime, or at the least no asymptotic value for the thermal conductivity with increasing chain length was identified in this work. Also, the question of thermal equilibrium in an asymmetric nonlinear system is a somewhat tricky point due to the possibility of significant hysteresis in the system. Once the diode oscillator is above the diode turn-on temperature, the coupling of energy into the diode rises significantly, so the temperature must be lowered well below this turn-on temperature to turn off the diode again. The study of thermally activated escape in the presence of such a "two-state" defect would be an interesting direction for future research.

The frequency dependence of flux through the defect indicates that the low thermal conductivity operation is due to phononic Rayleigh scattering. The finite depth and asymmetric coupling introduce a critical switch-on temperature for forward bias and a much higher breakdown temperature in reverse bias. This approach captures, in a simple way, the temperature-dependent thermal conductivity and asymmetric coupling underpinning thermal diode experiments, while the specific approach opens up a pathway for the design and implementation of thermal diode devices using a defect. The small scale of the defect relative to the phonon wavelength makes implementation in a solid-state environment challenging; however, in artificial crystalline structures with larger spatial scales, implementation looks more straightforward. Ion crystals [30] or trapped atom systems [31] are both possible pathways to test high thermal rectification effects mediated by a single defect.

There are a number of possible directions for further work. The influence of quantum effects on possible rectification behavior in the presence of a small scale defect could be examined; the results could be extended to higher-dimensional models; and the implications in other systems, such as implementations of acoustic or optical diodes, could be considered. Overall, the identification of the key mechanisms for diode behavior in this simple model opens up the possibility of diverse implementations of defect-mediated flow.

ACKNOWLEDGMENTS

The author thanks Stefano Lepri, Navneet Krishnan, Benjamin Fan, and Gaurav Agrawal for useful discussions.

[1] L. Yang, Z.-G. Chen, M. S. Dargusch, and J. Zou, Adv. Energy Mater. **8**, 1701797 (2018).
[2] W. Kim, R. Wang, and A. Majumdar, Nano Today **2**, 40 (2007).
[3] N. Roberts and D. Walker, Int. J. Therm. Sci. **50**, 648 (2011).
[4] N. Li, J. Ren, L. Wang, G. Zhang, P. Hänggi, and B. Li, Rev. Mod. Phys. **84**, 1045 (2012).
[5] *Thermal Transport in Low Dimensions*, edited by S. Lepri (Springer International Publishing, Switzerland, 2016).
[6] M. Terraneo, M. Peyrard, and G. Casati, Phys. Rev. Lett. **88**, 094302 (2002).
[7] B. Li, L. Wang, and G. Casati, Phys. Rev. Lett. **93**, 184301 (2004).
[8] B. Hu, L. Yang, and Y. Zhang, Phys. Rev. Lett. **97**, 124302 (2006).
[9] S. Chen, D. Donadio, G. Benenti, and G. Casati, Phys. Rev. E **97**, 030101(R) (2018).
[10] Z. Rieder, J. L. Lebowitz, and E. Lieb, J. Math. Phys. **8**, 1073 (1967).
[11] S. Lepri, R. Livi, and A. Politi, Phys. Rev. Lett. **78**, 1896 (1997).
[12] M. Pons, Y. Y. Cui, A. Ruschhaupt, M. A. Simón, and J. G. Muga, Europhys. Lett. **119**, 64001 (2017).
[13] A. Maznev, A. Every, and O. Wright, Wave Motion **50**, 776 (2013).
[14] E. Pereira, Phys. Rev. E **96**, 012114 (2017).
[15] G. Wu, Y. Long, and J. Ren, Phys. Rev. B **97**, 205423 (2018).
[16] D. Segal and A. Nitzan, Phys. Rev. Lett. **94**, 034301 (2005).
[17] D. Segal and A. Nitzan, J. Chem. Phys. **122**, 194704 (2005).
[18] C. W. Chang, D. Okawa, A. Majumdar, and A. Zettl, Science **314**, 1121 (2006).
[19] P. R. Gaddam, S. T. Huxtable, and W. A. Ducker, Int. J. Heat Mass Tran. **106**, 741 (2017).
[20] I. Kim, M. Kang, and S. W. Kim, Int. J. Thermophys. **38**, 172 (2017).
[21] S. Wang, A. L. Cottrill, Y. Kunai, A. R. Toland, P. Liu, W.-J. Wang, and M. S. Strano, Phys. Chem. Chem. Phys. **19**, 13172 (2017).
[22] L. Tang and M. Francoeur, Opt. Express **25**, A1043 (2017).
[23] O. M. Braun and Y. S. Kivshar, Phys. Rep. **306**, 1 (1998).

[24] S. Lepri, R. Livi, and A. Politi, Phys. Rep. **377**, 1 (2003).
[25] B. Li, J. H. Lan, and L. Wang, Phys. Rev. Lett. **95**, 104302 (2005).
[26] D. Hennig, C. Mulhern, L. Schimansky-Geier, G. Tsironis, and P. Hänggi, Phys. Rep. **586**, 1 (2015).
[27] M. J. Gillan and R. W. Holloway, J. Phys. C **18**, 5705 (1985).
[28] B. Hu, B. Li, and H. Zhao, Phys. Rev. E **57**, 2992 (1998).
[29] J. Schmidt, A. Lambrecht, P. Weckesser, M. Debatin, L. Karpa, and T. Schaetz, Phys. Rev. X **8**, 021028 (2018).
[30] N. Freitas, E. A. Martinez, and J. P. Paz, Phys. Scripta **91**, 013007 (2016).
[31] I. Bloch, Nat. Phys. **1**, 23 (2005).